Inferring Global Topology from Local Juxtaposition Geometry: Interlinking Polymer Rings and Ramifications for Topoisomerase Action

Zhirong Liu,* E. Lynn Zechiedrich,[†] and Hue Sun Chan*

*Department of Biochemistry, and Department of Medical Genetics and Microbiology, Faculty of Medicine, University of Toronto, Toronto, Ontario M5S 1A8, Canada; and [†]Department of Molecular Virology and Microbiology, Baylor College of Medicine, Houston, Texas 77030 USA

ABSTRACT   Lattice modeling is applied to investigate how the configurations of local chain juxtapositions may provide information about whether two ring polymers (loops) are topologically linked globally. Given a particular juxtaposition, the conditional probability that the loops are linked is determined by exact enumeration and extensive Monte Carlo sampling of conformations satisfying excluded volume constraints. A discrimination factor f_L, defined as the ratio of linked to unlinked probabilities, varies widely depending on which juxtaposition is presumed. $|\log f_L|$s that are large for small loop size n tend to decrease, signaling diminishing topological information content of the juxtapositions, with increasing n. However, some juxtaposition geometries can impose sufficient overall conformational biases such that $|\log f_L|$ remains significant for large n. Notably, for two loops as large as $n = 200$ in the model, the probability that passing the segments of a hooked juxtaposition would unlink an originally linked configuration is remarkably high, $\sim$85%. In contrast, segment-passage of a free juxtaposition would link the loops from an originally unlinked configuration more than 90% of the time. The statistical mechanical principles emerging from these findings suggest that it is physically possible for DNA topoisomerases to decatenate effectively by acting selectively on juxtapositions with specific "hooked" geometries.

INTRODUCTION

The study of topological entanglement, such as catenation and knotting, is a rigorous mathematical pursuit (1–3), and at the same time a subject of intense practical interest to many branches of science (4) and engineering (5). As far as chemical topology of molecular structures is concerned (6), topological constraints arise readily in ring polymers (7,8) as well as linear polymer melts (9). The properties of these configurational restrictions have a direct impact on polymer viscoelasticity (9,10) and the spatial extent of conformational fluctuations (11–13).

Many important biomolecules are polymers. Hence, questions about covalent topology are clearly relevant to molecular biology (14). For proteins, experimental data collected so far have indicated that topological entanglement is rare (15), though not nonexistent (16–20). In contrast, for DNA, it is well known that the formation of supercoils, catenanes, and knots are critical for its function or malfunction, and that potential problems associated with these topological features are prevalent (21,22). Under conditions of topological equilibrium (23–26), an ensemble of circular DNA molecules populates many states with different degrees and patterns of linking and knotting. DNA topoisomerases (27) are enzymes that change the topology of DNA by first cleaving a segment of the molecule (which can be either a single DNA strand or a DNA double helix), allowing the passage of another segment through the break thus created, and then resealing the transient break (28,29). Remarkably, a class of topoisomerases, designated type 2, because they change DNA linking number in steps of two and effect passage of segments of the DNA double helix, are found to have the ability to significantly lower the degrees of knotting and catenation among DNA molecules to a steady-state level well below their corresponding equilibrium values (30). This observation immediately raises intriguing questions as to how the recognition of the topological state of the DNA is achieved by the topoisomerase (31). Because the topoisomerase is much smaller than the DNA molecule it is acting on, it seems reasonable that the topoisomerase must be able to exploit spatially local properties of the DNA—albeit the extent of this "locality" may be an open question (see below)—to infer the topological state of the DNA. As such, biology is apparently offering a general, practical strategy for disentanglement that other lines of inquiry might not yet have come across. Thus, deciphering the physical basis of local inference of global topology is useful not only for understanding important cellular functions, but would likely lead to broader implications in other research areas as well.

Several hypothetical mechanisms have been proposed to rationalize the ability of type 2 topoisomerase to gather topological information from local binding events. These include a "three-binding-sites model", wherein the topoisomerase senses the topological state of the DNA by actively sliding along the DNA contour after first binding (30). Also proposed is a "kinetic proofreading model" in which two temporally separated topoisomerase-DNA collisions are required

to effect DNA segment passage, thus allowing certain spatially nonlocal conformational information to be sampled (32,33). A third mechanism, which may be termed the "active bending model", proposes that the topoisomerase actively deforms the DNA conformation at the binding site. According to the model, this process would lead to a topological bias when DNA passage through the deformed region is further restricted to be unidirectional (34,35). A fourth mechanism, referred to as the "three-segment interaction model", stipulates that a bound topoisomerase, essentially stationary with respect to the DNA, achieves topological bias by interacting with three DNA segments. In this way, its action would be based on presumably more topological information about the DNA molecule than that can be gleaned from a two-segment juxtaposition (36).

A simpler mechanism was proposed by Buck and Zechiedrich (37). It takes into account only the information provided by the local curvature and the relative orientation of the two segments making up a DNA juxtaposition. In this hypothesis, by virtue of the preferential binding of type 2 topoisomerases to DNA juxtapositions (38), the topological bias of the topoisomerase is achieved by acting selectively on preexisting "hooked" rather than "free" juxtapositions (37). Recent structural evidence from x-ray crystallography appears to support this view (39). Additional biological data are also best explained by this proposed mechanism (40). The primary concern of our work is more fundamental, however. Our aim is to examine, in large measure irrespective of experiment, whether the hypothesis is logically, mathematically, and physically possible; and if so, what are the quantitative implications of the proposed mechanism. For instance, if such an inference from local juxtaposition geometry to global topology can be achieved in some situations, how does the reliability of the inference depend on the size and shape of the polymeric conformations involved? Therefore, the central question we ask here is simple: given a particular juxtaposition geometry, how much can we infer about the global topology of the chain configurations? In other words, to what degree does substrate specificity for some particular juxtapositions represent the selection of chain configurations with certain topological biases? As a first step in this endeavor, we focus on a system of two ring polymers that can be either interlinked or not interlinked, as DNA catenanes (41,42) can be modeled rudimentarily as two interlinked polymer rings. Our analysis will be conducted in rather general terms using coarse-grained modeling. More detailed comparisons of our results to real molecular behavior may require structurally higher resolution models.

MODEL AND METHODS

Exact lattice enumeration

Lattice modeling is a coarse-grained approach to understanding polymer properties. Despite its apparent simplicity, lattice models have been tremendously useful for establishing general physical principles. Indeed, studies

based on exact enumeration of lattice conformations since the late 1940s (43–46) have led to important modern conceptual advances in polymer physics such as scaling theory (47) and renormalization group analyses (48). Lattice modeling has also been applied to knotting, with notable successes (1,13,49–51). In this study, we consider chains configured on three-dimensional simple cubic lattices. To account for the physical constraints of excluded volume, no configuration is allowed to have more than one monomeric unit ("bead") of the polymer from the same chain or from different chains to occupy the same lattice site. Ring polymers are thus modeled as self-avoiding lattice polygons.

Spatially local geometrical constraints on a polymer such as contacts or cross-links between different parts of the chain can result in significant biases in conformational distribution (52,53). Conversely, global conformational properties can have substantial impact on local geometry. In this connection, a notable observation from earlier exact lattice enumeration is that overall conformational compactness can enhance local preferences for helical and sheet-like structural motifs (53,54). Thus, the packing effects of compactness are seen as a significant driving force for secondary structure formation in globular proteins (55,56) and the preponderance of helices and sheet-like "planar zigzags" in crystals of synthetic polymers (57).

Pursuing a similar investigative logic, here we seek to determine how the constraints imposed by a given juxtaposition between two loops (three examples of which are shown in Fig. 1) may affect their topological distribution. A two-loop configuration is defined by the individual conformation of each of the two loops, and the relative translational and orientational separations between the two loops. For this purpose, we first use exact enumeration to construct two-loop configurations by "growing" from one end of each of the two segments of a given juxtaposition, and constrain the chain growing from each segment to form a loop by closing onto the other end of the given segment (see caption for Fig. 1). In other words, the starting point of our configurational analysis is a given juxtaposition geometry. This procedure allows us to determine the probabilities of different topological states (see below), conditioned upon the starting juxtaposition. Our logical reasoning differs from approaches that consider specific topological states as starting points of analyses. Thus, the present methodology is complementary to other pertinent lattice (49,50) and continuum (34,58) modeling efforts.

For any complete two-loop configuration generated by exact enumeration using the above-described growth procedure, the linking number, Lk, between the two lattice loops is determined using the algorithm of Fourey and Malgouyres (59) from the coordinates of the chains. Consideration of this Lk is appropriate for catenation as it accounts only for the linkage (or lack thereof) between the two loops without regard to the topological complexity of individual loops. In using this Lk, it should be noted that whereas all unlinked configurations have $Lk = 0$ (i.e., all $Lk \neq 0$ configurations are
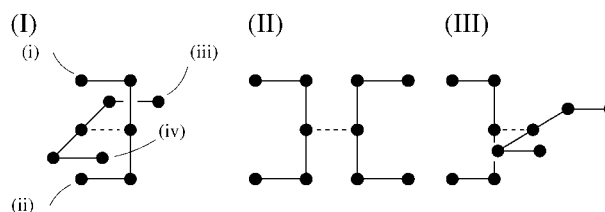

FIGURE 1 Three special 5 mer-on-5 mer juxtapositions configured on the simple cubic lattice: (I) hooked, (II) free (planar), and (III) free (nonplanar). They will be referred to by these labels throughout this study. Besides these three, many other juxtaposition geometries are possible in our model (Table 1). For every such juxtaposition, the middle positions of the two polymer chain segments are required to be nearest lattice neighbors (indicated by *dashed lines* connecting the two middle *beads* for the examples shown). Two-loop configurations are constructed by joining points *i* and *ii* with a self-avoiding lattice walk to form one ring polymer, and by joining points *iii* and *iv* by another self-avoiding walk to form a second ring polymer. To enforce excluded volume, every site on the lattice is not allowed to be occupied by more than one polymer element.

linked), some $Lk = 0$ configurations, such as those with a Whitehead's link (59), can be linked. Nonetheless, for the loop sizes considered in this study, linked configurations with $Lk = 0$ constitute only a very small fraction of all $Lk = 0$ configurations. (In this study, the ''size'' of a loop refers to the number of beads that make up the loop.) Hence, while not losing sight of this intricacy, for terminological simplicity we will simply refer to our $Lk = 0$ and $Lk \neq 0$ two-loop configurations, respectively, as unlinked and linked.

Table 1 shows that the diversity of juxtaposition geometries depends on the numbers of beads of the two segments defining the juxtaposition. To provide sufficient coverage of subtle geometrical effects that can only be captured by lattice chain segments with more beads, yet at the same time keep our modeling exercise computationally tractable, here we choose to be concerned only with the 5 mer-on-5 mer (5, 5) juxtapositions (five beads for each segment). Each 5 mer segment can take 15 different shapes. The combination of pairs of such segments at different relative orientations leads to a fairly large number of different juxtaposition geometries. The hooked and free juxtapositions in Fig. 1 are three among a total of 2,982 such juxtapositions, from which two-loop configurations are constructed. In this study, we focus mainly on cases when the two loops are of the same size, denoted as n (n is the number of beads). As an illustration of the lattice method, an example $Lk = 2$ two-loop configuration obtained by exact enumeration is depicted in Fig. 2.

Monte Carlo sampling

By accounting for all possible two-loop configurations, exact conformational enumeration provides exhaustive information about their topological linkage. However, because the number of configurations, and thus the time needed for computation, increases exponentially with loop size n, for loops larger than that in Table 2, exact enumeration would fast become computationally impractical. To extend our analysis to a broader range of loop sizes, we adopt the Monte Carlo algorithm of Madras et al. (60). In this algorithm, the size of each loop is constant, always kept at the given (input) value. Starting with any loop conformation, new loop conformations are generated by a move set consisting of three types of chain moves: inversion, reflection, and interchange transformations, as defined in the original reference (60). These moves permit conformational transitions between dif-

TABLE 1 Number of distinct simple cubic lattice configurations of two chain segments whose middle positions, one from each chain segment, are constrained to be nearest neighbors on the lattice

Numbers of beads in the two segments	Number of distinct juxtaposition geometries
1, 1	1
3, 3	13
5, 5	2,982
7, 7	1,243,223
9, 9	570,194,001
1, 3	3
3, 5	293
5, 7	118,317
7, 9	52,955,213
9, 11	24,332,981,086

Configuration counts are obtained by exact enumeration. The numbers tabulated here are for distinguishable configurations (distinct shapes) not related to one another by translational, rotational, and inversion operations on the lattice, nor are they related by symmetry operations of swapping the two chain segments and/or reversing the contour direction of the chain sequence of individual segments. This study focuses on the 5 mer-on-5 mer (5, 5) juxtapositions because they provide geometric diversity yet are computationally tractable. The juxtapositions in Fig. 1 are three special examples among 2982 possible (5, 5) juxtaposition geometries.
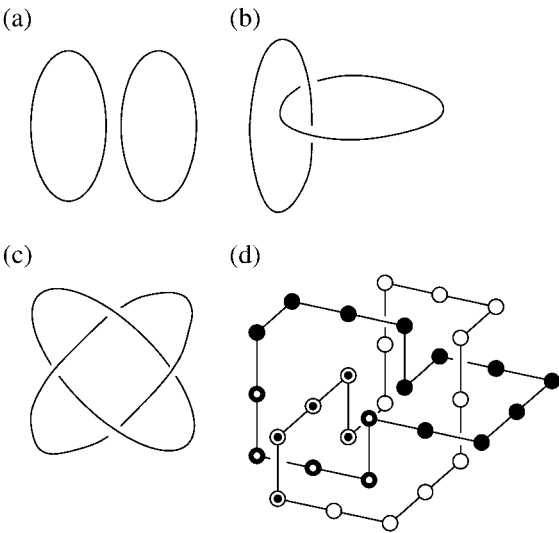
FIGURE 2   Schematics of two-loop configurations with different linking numbers Lk: (a) $Lk = 0$, (b) $Lk = 1$, and (c) $Lk = 2$. (d) Drawing of a lattice realization of two $Lk = 2$ loops with sizes $n = 16$. Lattice sites along the two different loops are represented, respectively, by white and black beads. Ten lattice sites constituting a hooked juxtaposition are marked by center black dots for the white beads and center white dots for the black beads. To elucidate the decatenation action of type 2 topoisomerases, the lattice chains here may be viewed as a model for the DNA double helix. This treatment does not address the internal structure of the DNA double helix, i.e., single-strand DNA is not considered. Accordingly, it should be noted that the loop-linking number Lk in this study does not correspond to the linking number defined for individual DNA strands.

ferent topological states, and ensure ergodic sampling. In other words, chain segments can ''pass through'' one another during the moves, but the end product of each move, i.e., the new configuration, is not allowed to violate excluded volume (see below). Each of these moves is initiated by first identifying randomly a pair of loop positions, or beads. For each loop, all possible bead pairs have equal chance to initiate a chain move, except for the inner beads of the fixed juxtaposition. The only beads in the juxtaposition allowed to initiate a chain move are the four endpoints of its two segments. A list is made of all possible conformational transformations defined by the given bead pair. Then, a transformation is randomly chosen from the list to generate a putative new conformation, also termed the attempted move, which is accepted if it does not violate excluded volume constraints. Otherwise, it is rejected, in which case the original unchanged conformation contributes one more time to the sample. The two-loop linking number Lk is determined as before (59). This process is then repeated until sufficient conformational sampling has been performed to ensure convergence, i.e., when the variations of the computed averages of the quantities of interest are negligible. We have carried out this procedure for loop sizes as large as $n = 200$. The ratios of the number of accepted chain moves to the number of attempted moves are reasonable. For example, these ratios are ~0.41, 0.36, 0.30, and 0.26, respectively, for the $n = 24$, 50, 100, and 200 simulations. Thus, conformational sampling is efficient for the loop sizes we considered.

RESULTS AND DISCUSSION

Configurational counts and topological discrimination factors

We begin with the hooked juxtaposition and two free juxtaposition geometries in Fig. 1. We pay special attention to the

TABLE 2 Number of two-loop configurations with a preformed juxtaposition, as a function of loop sizes and linking number, *Lk*, that measures the degree of linking between the two loops

	Hooked juxtaposition (I)			Free juxtaposition (II)		Free juxtaposition (III)	
Loops of equal size, n	$Lk = 0$	$Lk = 1$	$Lk = 2$	$Lk = 0$	$Lk = 1$	$Lk = 0$	$Lk = 1$
8	0	1	0	81	0	81	0
10	0	729	0	12,321	0	12,321	0
12	16	219,636	0	2,164,122	0	2,125,764	0
14	63,265	61,603,012	0	474,700,624	4	458,702,508	0
16	52,976,204	17,868,898,017	868	119,888,519,057	12,132,856	114,797,003,485	7,944,384
Loops of different sizes							
8, 10	0	27	0	999	0	999	0
10, 12	0	12,702	0	163,322	0	161,838	0
12, 14	1,249	3,688,442	0	32,062,976	0	31,232,932	0
14, 16	1,832,245	1,051,318,734	0	7,547,091,984	348,364	7,259,078,100	231,100
16, 18	1,257,668,570	311,219,768,134	282,634	1,995,862,293,320	380,299,806	1,906,252,766,102	277,398,133

The three juxtapositions I, II, and III correspond to the ones depicted in Fig. 1. The tabulated numbers are obtained by exact enumeration on simple cubic lattices. Each count corresponds to the number of two-loop configurations consistent with the existence of the given juxtaposition at a fixed position and orientation. The counts do not include any translational, rotational, or inversion transformation of the starting juxtaposition.

hooked and free juxtapositions because intuitively they correspond to rather extreme local geometric and steric constraints with likely opposite topological effects (37). For this purpose, juxtaposition (I) with a 90° cross angle between the two segments is chosen because it is the only fully hooked geometry among all (5, 5) juxtaposition geometries (Table 1). For free juxtapositions, (II) and (III) with different segment cross angles (0° and 90°) are possible. Thus, results from these two geometries are expected to be useful for delineating possible angular effects among free juxtapositions. Table 2 gives the numbers of linked and unlinked two-loop configurations containing these three juxtapositions that we have determined using the exact enumeration method. Accordingly, each set of configurations in the table may be viewed as corresponding to a subset of all possible two-loop configurations in topological equilibrium (23,25,26), where the subset is being defined by the restriction that there is at least one incidence of the given juxtaposition in the configuration.

Table 2 shows that the hooked juxtaposition behaves very differently from the two free juxtapositions with respect to the distribution of topological states among the two-loop configurations. For the hooked juxtaposition (I), most of the implied configurations are linked. Indeed, for small loop sizes, $n = 8$ and $n = 10$ for example, it is impossible to have this hooked juxtaposition without having the two loops being linked, a fact that is intuitively obvious from a simple inspection of the cubic lattice geometry. For larger loop sizes, Table 2 indicates that this hooked juxtaposition can be consistent with unlinked configurations, but their numbers are much smaller than that of the linked conformations. At the same time, when the loop sizes are larger ($n \geq 16$), it is possible for the two loops to be doubly linked ($Lk = 2$) if there is a hooked juxtaposition between the two loops.

The corresponding behavior of the two free juxtapositions are opposite to that of the hooked juxtaposition. For small loops ($n \leq 12$), no linked configuration can be consistent

with either free juxtaposition. For larger loops, linked configurations are possible, but their numbers are much smaller, consistently, than that of the hooked juxtaposition. For the loop sizes in Table 2, the maximum degree of linkage between two loops with a preformed free juxtaposition (II or III) is $Lk = 1$, which is lower than the $Lk = 2$ value possible for $n \geq 16$ loops with a preformed hooked juxtaposition.

With the configuration counts, the probabilities that a given juxtaposition is part of a linked two-loop configuration, or part of an unlinked two-loop configuration, can be computed readily. As discussed above, these probabilities are based on an underlying sample space of configurations in topological equilibrium. Let Ω_0 be the total number of configurations, and Ω_L be the number of linked configurations, both subject to the constraint of having a given juxtaposition. Then the probability, conditioned upon the given juxtaposition, that the two loops are linked is Ω_L/Ω_0, and the corresponding conditional probability that the two loops are not linked is $1 - \Omega_L/\Omega_0$. For instance, for two loops of size $n = 16$, the conditional probability that a two-loop configuration with a hooked juxtaposition is linked is $(17,868,898,017 + 868)/(52,976,204 + 17,868,898,017 + 868) \approx 99.7\%$, whereas the corresponding conditional probabilities that a two-loop configuration with a free juxtaposition (II or III) are linked are, respectively, $12,132,856/(119,888,519,057 + 12,132,856) \approx 0.01\%$ or $7,944,384/(114,797,003,485 + 7,944,384) \approx 0.007\%$. This means that if a hooked juxtaposition is observed between two $n = 16$ loops, it is almost certain that the two loops are linked. On the other hand, if a free juxtaposition is observed between the same two loops, it is almost certain that they are not linked. These extreme probabilities, at least for relatively small loop sizes $n = 8$–16, indicate that knowledge about preexisting juxtapositions can, in principle, be used statistically to discriminate the underlying topological state of the configuration. Therefore, we find it useful to define a discrimination factor,

$$f_L = \frac{\Omega_L}{\Omega_0 - \Omega_L}, \qquad (1)$$

which is equal to the ratio of conditional probabilities that the two loops are linked versus that they are not linked. For example, for two loops of size $n = 16$ and juxtapositions I, II, and III, respectively, $f_L = 333.7$, 1.0×10^{-4}, and 6.9×10^{-5}. Hence, this factor is a measure of the topological information content of a given juxtaposition. A high (or low) f_L value implies that it is much more (or less) probable for the two-loop configuration with the given juxtaposition to be linked rather than not linked. In this way, f_L provides a means to assess reliability when an inference based on a given juxtaposition is made about the topological state of the global configuration. Further specifications may be applied to the configuration counts in Eq. 1, for example, by restricting the counts to configurations with a certain characteristic, to examine how the topological information content of a juxtaposition may vary depending on the underlying configurational space of interest (see below).

Fig. 3 studies in some detail how the discrimination factor of the hooked juxtaposition depends upon the intra- and interloop contacts. A contact is defined by a pair of nearest lattice neighbors between two polymer beads that are not sequential along the contour of a chain. As the number of intraloop contacts is a direct measure of the compactness of a conformation (53), the results from this study are relevant to questions about how the overall compactness of the individual loops and other conformational features related to contact formation may impact the topological discriminating power of specific juxtapositions. Fig. 3 shows that f_L exhibits significant variations as a function of the two numbers of intraloop contacts. Whereas the overall f_L is ~ 340 (see above), Fig. 3 a indicates that f_L is much higher at ≈ 2000 for the subset of two-loop configurations with essentially no intraloop contacts ($q_{11} \approx q_{22} \approx 0$). This quantitative result echoes the argument made previously by Buck and Zechiedrich (37) that hooked juxtaposition invariably implies linkage for perfect circles. Small lattice loops with no intraloop contacts are intuitively similar to small circles (that also have no intraloop contacts by definition) in certain geometrical respects (cf. the $n = 8$ case discussed above). Therefore, it is not too surprising that f_L is higher for this class of lattice configurations. What is surprising is the magnitude of the effect.

Interestingly, the $n = 16$ result in Fig. 3 a shows that there is a local maximum with $f_L \approx 1200$ on the q_{11}–q_{22} plane when $q_{11} \approx q_{22} \approx 3$. For loop size $n = 16$, the maximum possible number of intraloop contacts is seven. Thus, this trend suggests that the topological discrimination power of the hooked juxtaposition can be increased substantially if the two loops are both constrained to form an intermediate number, approximately midway between zero and the maximum possible number, of intraloop contacts. We will examine further this intriguing phenomenon and its possible experimental implications in the next subsection. Here, Fig. 3 b shows that f_L decreases sharply and essentially monotonically with increasing number of interloop contacts (q_{12}) or increasing overall compactness of the two-loop configuration (as measured by q). In particular, when the two $n = 16$ loops are constrained to have the maximum possible number of interloop contacts, the hooked juxtaposition would essentially lose its power to discriminate between linked and unlinked two-loop configurations ($\log f_L \approx 0$, i.e., $f_L \approx 1$ for $q_{12} \approx 24$–27). Taken together, the results in Fig. 3 underscore the important role of contact pattern of the underlying global configuration in enhancing or diminishing the reliability of topological inference from local juxtapositions.

Effects of system size on the implied topological bias of a juxtaposition

The above analysis shows that the three juxtapositions in Fig. 1 impose impressive topological biases on relatively small loops. For the loop sizes in Table 2, the discrimination factor f_L is either very high or very low (i.e., the absolute value $|\log f_L|$ is high, $|\log f_L| \to \infty$ for the smaller loops). However, as topological diversity increases with loop size, the trend in Table 2 indicates that f_L would take less extreme values as the loop size increases. To ascertain whether the topological discriminating power of the juxtapositions remains significant for larger loops, Monte Carlo sampling is used to extend the study to loops with as large as 200 beads (Fig. 4). To test the validity of the Monte Carlo procedure, we calculated the Monte Carlo f_L for $n = 16$ for the three juxtapositions and the f_L for $n = 12$ for the 1 mer-on-1 mer control case in Fig. 4. The Monte Carlo results are practically indistinguishable from the corresponding discrimination factors computed from exact enumeration data.

As expected, Fig. 4 shows that $|\log f_L|$ decreases with increasing loop size n: As n increases, the f_L factor for the hooked juxtaposition decreases from its high values for small n, whereas the f_L factors for the two free juxtapositions increase from their low values for small n. The behavior of the two free juxtapositions are very similar. Their $\log f_L$ values are practically indistinguishable for $n \geq 50$. Nonetheless, for small loop sizes, the nonplanar free juxtaposition (III) is noticeably more biased against linked configurations than the planar free juxtaposition (II), as is evident from the lower $\log f_L$ values for the former (Fig. 4, *triangles*) that for the latter (*squares*) for $n \leq 34$ (cf. the corresponding $n = 14$ and 16 data in Table 2). These observations suggest that the topological constraints imposed by these two free juxtaposition geometries are very similar, and that the differences of their effects are spatially local in character.

The most interesting observation here, however, is that the f_L factors in Fig. 4 do not appear to asymptotically approach $\log f_L = 0$, or $f_L = 1$. Instead, apparently, $\log f_L$ for the hooked juxtaposition tends to a positive value; on the other hand, the essentially equal $\log f_L$ for the two free
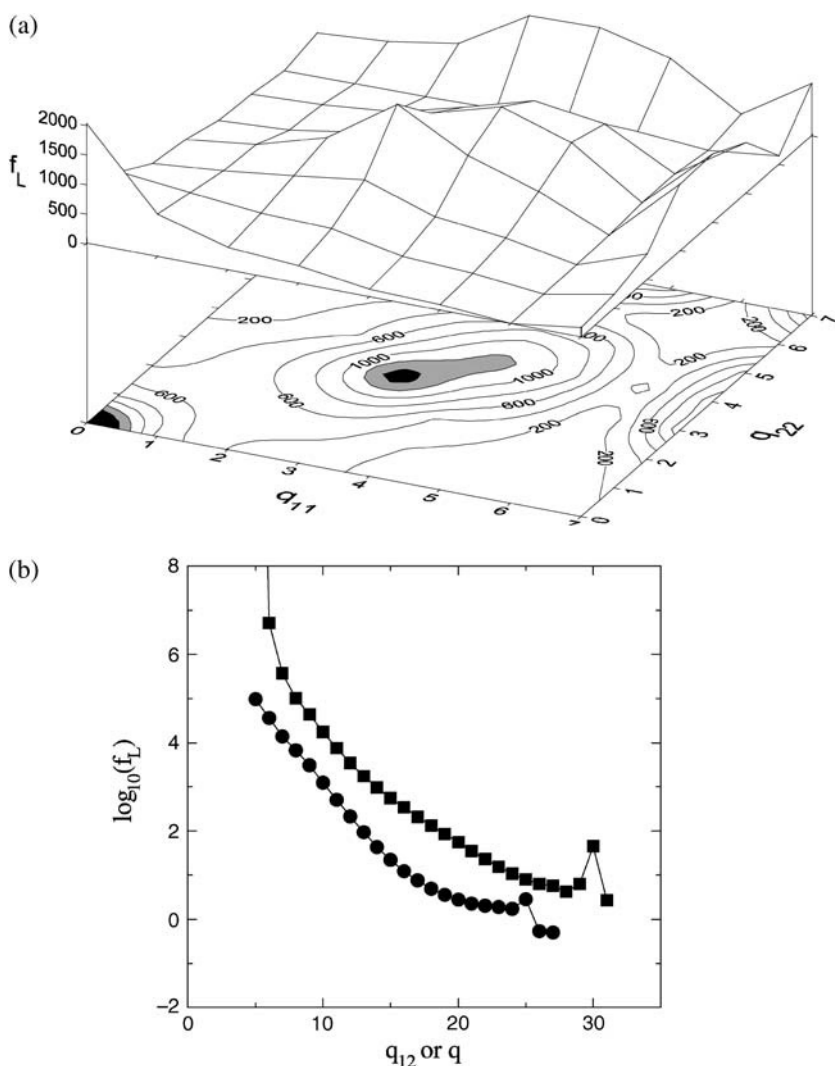
(a)

(b)

FIGURE 3 Discrimination factor f_L (ratio of linked/ unlinked number of configurations) of the hooked juxtaposition (Fig. 1, I) is determined by exact enumeration for two $n = 16$ loops. (a) f_L as a function of the number of intraloop contacts within one (q_{11}) and the other (q_{22}) loops. f_L is defined only at integer values of q_{11} and q_{22}. The contour plot is constructed by interpolation for illustrative purposes. Areas on the q_{11}–q_{22} contour plot with highest values of f_L are highlighted by shading: $1200 < f_L < 1400$ is in gray, and $1400 \leq f_L < 1600$ is in black. (b) f_L as functions of the number of interloop contacts q_{12} (●) or the total number of contacts q (■, $q = q_{11} + q_{12} + q_{22}$). Line segments joining data points are merely a guide for the eye. The minimum possible value of q is 5 because there are 5 interloop contacts in the hooked juxtaposition to begin with. Because there is no unlinked configuration for $q = 5$ when $n = 16$, $\log f_L(q = 5) \rightarrow \infty$.

juxtapositions tends to a negative value. In other words, these juxtapositions do not become equivocal about the topological state of their underlying configurations. The existence of one of these juxtapositions in a two-loop configuration can still provide significant topological information even when the loop sizes are large. For loop size $n = 200$, $\log_{10} f_L \approx 1$ for the hooked juxtaposition, meaning that even for this large loop size, it is still ~10 times more likely that an $n = 200$ two-loop configuration underlying a hooked juxtaposition is linked rather than not linked. For the same loop size, $\log_{10} f_L \approx -1$ for the free juxtapositions, implying that the topological distribution of the underlying two-loop configurations for the free juxtapositions is essentially opposite that of the hooked juxtaposition. For the free juxtapositions, the configurations are ~10 times more likely to be not linked than linked. These observations suggest strongly that the local distinctions of these juxtapositions, their particular bond and torsional angles, etc., amount to a kind of intrinsic background conformational bias with topological consequences that cannot be obviated by increasing loop size.

Fig. 4 considers also the f_L values for a 1 mer-on-1 mer (1, 1) juxtaposition as a control case (*diamonds*). Similar to the two free juxtapositions, the log f_L values for this control case are negative, indicating a bias against linked configurations, but this bias is less strong (less negative log f_L) for the (1, 1) juxtaposition than for the two free juxtapositions. The variation of log f_L with n for the (1, 1) juxtaposition exhibits a trend similar to that of the two free juxtapositions, and the difference in f_L between the (1, 1) and the two free juxtapositions narrows as n increases. Because the (1, 1) juxtaposition embodies no local juxtaposition geometry, its negative log f_L values imply that, if local juxtaposition geometry is disregarded, on average the mere existence of a juxtaposition constitutes a topological bias favoring unlinked configurations.

Fig. 5 investigates how f_L of the hooked juxtaposition depends on the numbers of intraloop contacts, and thus compaction, for larger loops. Comparing these results for $n = 50$ and 100 with that for the smaller loop size $n = 16$ in Fig. 3 a shows differences as well as similarities in the pattern
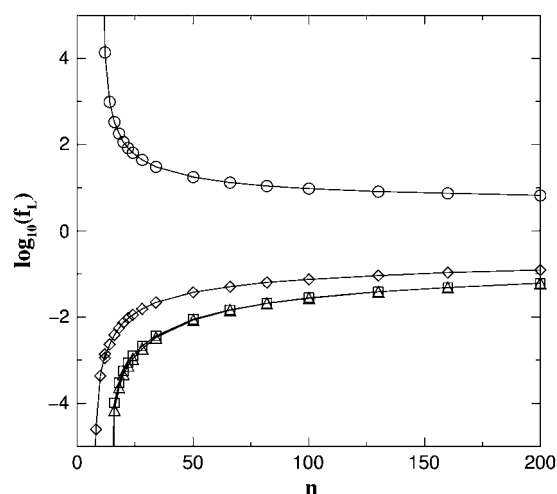
FIGURE 4 Discrimination factors f_L of the juxtapositions in Fig. 1 as functions of loop size n. Circles, squares, and triangles are, respectively, data points for the (I) hooked, (II) free (planar), and (III) free (nonplanar) juxtapositions in Fig. 1. Included for comparison is f_L for a control situation ($\diamond$) in which a pair of positions, one from each of the two loops (satisfying excluded volume conditions as before), are nearest neighbor on the lattice, but otherwise are not constrained. Thus, the diamonds in the plot correspond to the discrimination factor for a 1 mer-on-1 mer juxtaposition. In these plots, curves through the data points are a guide for the eye. Data for $n \leq 16$ for the three 5 mer-on-5 mer juxtapositions and data for $n \leq 12$ for the control are obtained by exact enumeration. Corresponding data for $n \geq 16$ and $n \geq 12$ are obtained by Monte Carlo sampling, with the number of attempted chain moves for each data point varying from 3×10^9 to 1.8×10^{10}.

of variation of the hooked f_L with respect to q_{11} and q_{22}. For the small loop $n = 16$ cases, $q_{11} \approx q_{22} \approx 0$ is associated with exceptionally high f_L values (Fig. 3 a), but this is not the case for the larger loops in Fig. 5. Apparently, when the loop size is larger, the conformational freedom of an individual loop is large even for loops without intraloop contacts. In this case, such loops do not necessarily resemble perfect circles. Thus, configurations for two large loops with $q_{11} \approx q_{22} \approx 0$ are much less constrained by the initial hooked juxtaposition, and, therefore, provide less topological information than when the loops are smaller.

A conspicuous feature in the small-loop result in Fig. 3 a and the larger-loop results in Fig. 5 is that the discrimination factor f_L for the hooked juxtaposition is significantly enhanced for two-loop configurations that have intermediate numbers of intraloop contacts in both loops. Comparing Fig. 5 against Fig. 3 a shows that this effect is more prominent for larger loop sizes. For the $n = 16$ case in Fig. 3 a, f_L attains relatively high values around a local maximum for a very small range of intermediate q_{11} and q_{22} values. However, for each of the $n = 50$ and 100 cases in Fig. 5, a ridge of high f_L factors extends over a much larger regime of intermediate q_{11}, q_{22} values. At least for $n = 50$, the ridge apparently encompasses configurations with one (but not both) of the individual loops being almost maximally compact (q_{11} or q_{22} close to the maximum possible value for the given loop size).

The f_L values along the ridge is higher than that for other parts of the q_{11}–q_{22} plane as well. This behavior leads us to speculate that perhaps a certain level of intraloop contact formation may serve to decrease the effective loop size and therefore entail larger discrimination factors (cf. Fig. 4).

The statistical mechanical trend emerging from Figs. 3 a and 5 about intraloop contacts is relevant to the experimental observation that the decatenating action of type 2 DNA topoisomerases is more effective when the DNA molecules are supercoiled (41,42,61). Although supercoiling of individual loops is not monitored in this study, supercoiling inevitably leads to intraloop contacts. Supercoiling is expected to correspond to an intermediate number of intraloop contacts; this is in contrast to a maximal or near-maximal number of intraloop contacts that implies a globular overall shape (53) for the individual loop. Hence, if we assume that topoisomerase decatenates by acting selectively on hooked juxtapositions (37), increased decatenating effectiveness with supercoiling is rationalizable in our model by a significant enhancement of the topological discrimination factor f_L at an intermediate level of intraloop contact formation (Fig. 5). According to our polymer model, the topological bias imposed by a hooked juxtaposition in favor of linked configuration is higher if each loop of the underlying two-loop configuration is of intermediate compactness. This perspective is consistent with a similar, though less quantitative, argument advanced previously (37).

Probabilities of decatenation by segment passage

The significant and essentially opposite topological biases of the hooked and free juxtapositions observed above imply that a topoisomerase-like process of segment passage at these juxtapositions would most likely, respectively, disentangle (unlink) or entangle (link) the two ring polymers. We now address the operational question of disentanglement directly. We do so by considering ''virtual segment passages''. Here, a virtual segment passage of a juxtaposition is defined as an interchange of positions of the center beads, one from each of the two segments that make the juxtaposition; the two loops are then rerouted through the new, interchanged positions of the center beads at the juxtaposition (Fig. 6, *top panel*). In this way, the juxtaposition geometry is changed whereas the rest of the two-loop configuration and its overall shape remain unperturbed. Taken literally, this procedure would lead to bonds connecting second nearest lattice neighbors, and thus the resulting configuration would no longer belong to the set of allowed configurations in the simple cubic lattice model. But these segment-passage operations are ''virtual'' because they are only carried out hypothetically for the benefit of calculating the resulting change in Lk. We devise this method of analysis because it is a conceptually clear and computationally efficient way to explore the consequences of topoisomerase-like action in this model.
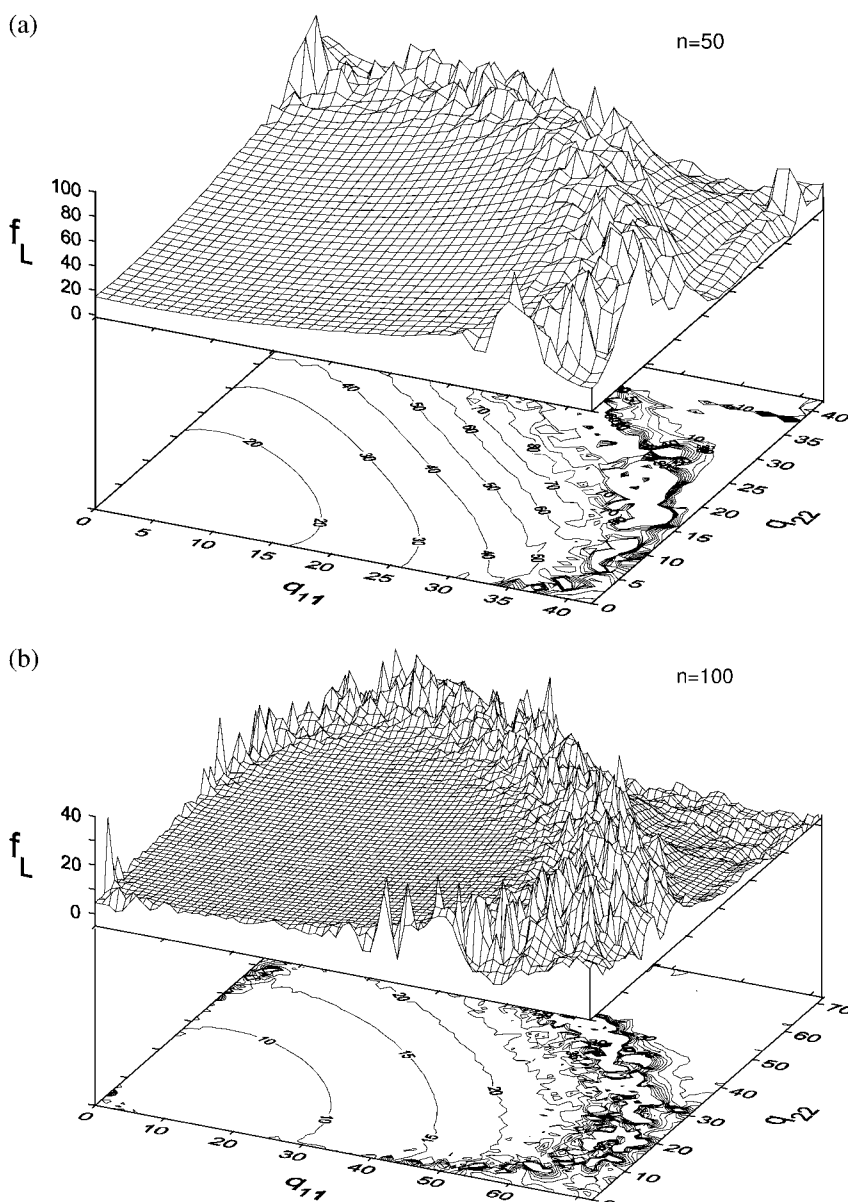
(a)

(b)

FIGURE 5 Discrimination factors of the hooked juxtaposition. Same as Fig. 3 but for larger loop sizes $n = 50$ (a) and $n = 100$ (b). Instead of using the exact enumeration method in Fig. 3, f_L values in this figure are computed by Monte Carlo sampling from a total of 1.02×10^{12} and 4.2×10^{11} attempted chain moves, respectively, for $n = 50$ and $n = 100$. It should be noted that only q_{11} and q_{22} values that have been sampled are shown in these plots. Some large values of q_{11} and q_{22} were not encountered in the simulation because their probabilities are very small. The maximum possible values for either q_{11} or q_{22} are ≈ 58 for $n = 50$ and ≈ 136 for $n = 100$. The numbers 58 and 136 are the maximum possible numbers of contacts, respectively, for linear chains (53) with 50 and 100 beads. These numbers are upper bounds on the number of intraloop contacts here because for a given number of beads, any collection of loop conformations is a subset of all possible linear chain conformations.

Fig. 6 shows the topological changes resulting from performing virtual segment passages on the hooked juxtaposition (I) and free juxtaposition (III). We do not apply virtual segment passage to juxtapositions with adjacent parallel bonds connected to the center beads of the two segments, e.g., free juxtaposition (II), because such a transformation does not mimic topoisomerase action and would also lead to apparent excluded volume clashes between the transformed bonds. The results in Fig. 6 confirm the strong statistical biases that are already obvious from the above discrimination factor considerations. When a hooked juxtaposition undergoes a segment passage, the probability that the process would decatenate two loops that were originally linked is extremely high (Fig. 6, *left*, *linked → unlinked panel*). As expected, this probability is attenuated by increasing loop size n. But even for loops as large as $n = 200$, the probability of decatentation is ~85%. This means that if a hypothetical topoisomerase only acts selectively on this hooked juxtaposition in the model, >85% of the time it would result in decatenation of two originally linked $n = 200$ loops, though it is possible (~13%) that such a segment passage would result in the catenation of two originally unlinked loops (Fig. 6, *left*, *unlinked → linked panel*). This bias is even stronger for smaller loops. If the two loops have $|Lk| > 1$ to begin with, Fig. 6 shows that segment passage of a hooked juxtaposition (that changes Lk by one unit) is approximately 10 times more likely to decrease linkage than to increase linkage between the loops (*linked → decreased linking*, and *linked → increased linking panels* on the *left*). In contrast, the effects of segment passage for a free juxtaposition are almost exactly the opposite.
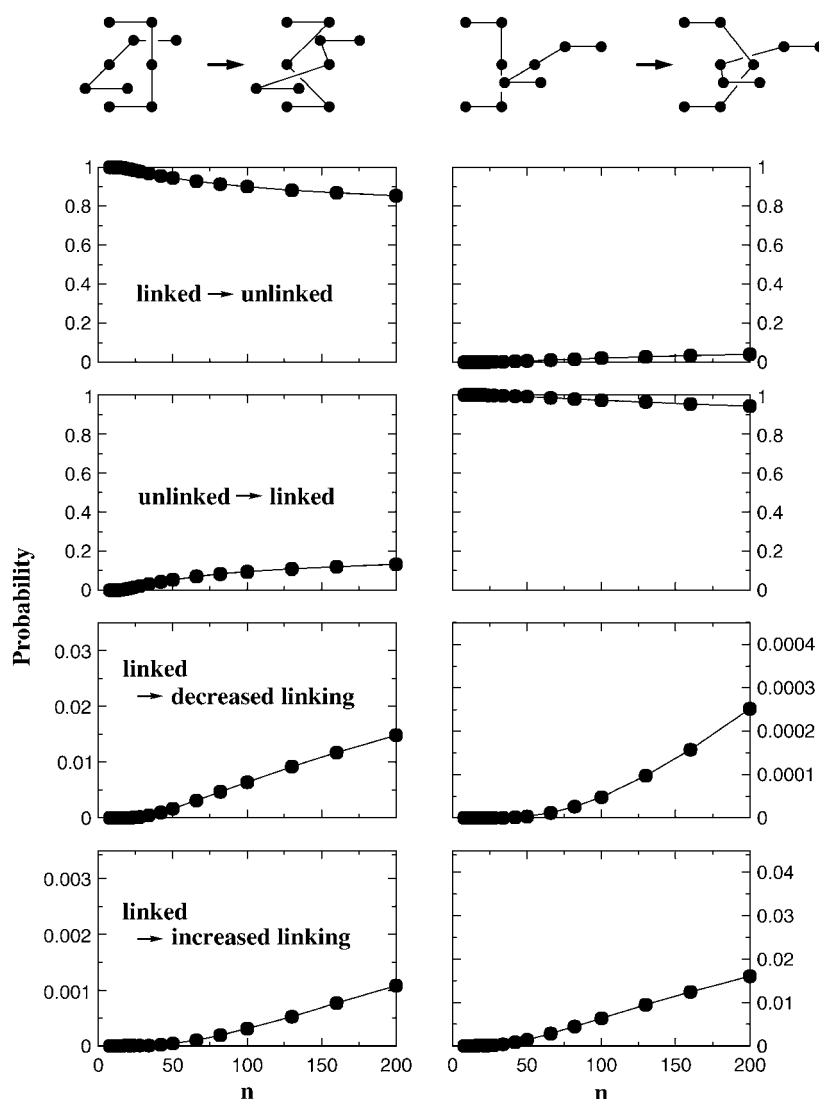
FIGURE 6 Changes of the linked/unlinked status of two-loop configurations caused by segment passage of different juxtapositions. The top graphics illustrate virtual segment-passages for a hooked (I) and a free (nonplanar, III) juxtaposition in the model. For each configuration obtained by exact enumeration or Monte Carlo sampling, a virtual segment passage operation at the given juxtaposition is performed to determine the resulting change in Lk. Four consequences of such topoisomerase-like processes are distinguished: i), a linked configuration becomes unlinked; ii), an unlinked configuration becomes linked; iii), the absolute value of the linking number of an originally linked configuration decreases, but the two loops remain linked; and iv), the absolute value of the linking number of a linked configuration increases. The probabilities of these four different outcomes are computed as functions of loop size n for an initially hooked (panels and scales on the left) or free (panels and scales on the right) juxtaposition. Since i–iv cover all possibilities, the probabilities for a given n along each vertical column add up to unity. Data for $n \leq 16$ are obtained by exact enumeration; those for $n \geq 16$ are from Monte Carlo sampling, where the number of attempted chain moves for each data point varies from 3×10^9 to 1.8×10^{10}. The maximum Lk encountered in our Monte Carlo simulations for the $n = 200$ loops here is $Lk = 4$ for the hooked juxtaposition and $Lk = 3$ for the free juxtaposition.

For instance, passing the two segments of a free juxtaposition (III) in the model would result in the catenation of two originally unlinked $n = 200$ loops >90% of the time (right column of Fig. 6). Again, this bias, which is opposite to that of the hooked juxtaposition, is even stronger for smaller loops. These model results suggest that, as has been proposed for DNA disentanglement by type 2 topoisomerase (37), selective segment passage of hooked juxtapositions can be an effective general mechanism to decatenate interlinked ring polymers.

We reemphasize that the probabilities of various topological states conditioned upon a presumed juxtaposition, as have been calculated in this work, are designed to address issues quite different from those addressed by the probabilities of occurrence of various juxtapositions conditioned upon a given topological state (34,62). The critical questions addressed by the conditional probabilities and f_L here are that of specificity: assuming that type 2 topoisomerases act selectively on juxtapositions with a specific geometry, how much

topological information can be offered by that juxtaposition and what is the probability of successful disentanglement by segment passage? The discussion above indicates that so far the answers to these questions are encouraging to the view that significant topological information is embodied in certain local juxtaposition geometries (37). On the other hand, under the same assumption about topoisomerase action, the conditional probability of occurrence of a specific juxtaposition geometry among loop configurations with a given underlying topology is related to the probability of enzyme-DNA binding and thus the efficiency of topological transformation and steady-state population distribution.

A general account of juxtaposition geometry and specificity of topological discrimination

To explore a broader context for the above consideration of the three representative juxtapositions in Fig. 1, it is instructive
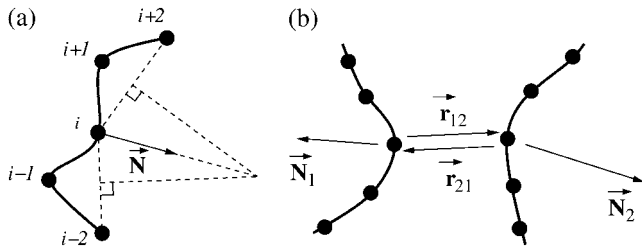
FIGURE 7 Schematics of a coarse-grained analytical description of juxtaposition geometry. (*a*) The curvature vector $\vec{N}$ of a 5 mer chain segment in this model is determined by the $i - 2$, i, and $i + 2$ positions: If $i - 2$, i, and $i + 2$ are collinear, $\vec{N} = 0$. Otherwise, perpendicular bisectors of the line segment from i to $i + 2$, and of the line segment from i to $i - 2$ are constructed on the plane defined by $i - 2$, i, and $i + 2$. The radius of curvature R (notation not shown in the figure) is the magnitude of the vector from position i to the intersection point of the two perpendicular bisectors. $\vec{N}$ shares the direction of this vector but with $1/R$ as its magnitude. (*b*) The vectors $\vec{N}_1$ and $\vec{N}_2$ are the curvature vectors of two 5 mer polymer chain segments that make up a juxtaposition; $\vec{r}_{12}$ is the vector from the central position of the first 5 mer to the central position of the second 5 mer, and $\vec{r}_{21} = -\vec{r}_{12}$. Two scalar parameters are defined to characterize juxtaposition geometry in this study: $\vec{N}_1 \cdot \vec{N}_2$ and $H \equiv \vec{N}_1 \cdot \vec{r}_{12} + \vec{N}_2 \cdot \vec{r}_{21}$ (see text for further details).

to take a more panoramic view of the relationship between juxtaposition geometry and topological bias. To this end, we now consider all 2,982 5 mer-on-5 mer juxtapositions (Table 1). Fig. 7 defines two scalar parameters, $\vec{N}_1 \cdot \vec{N}_2$ and H, for the general geometrical characterization of these juxtapositions in terms of the curvature vectors $\vec{N}_1$ and $\vec{N}_2$ at the
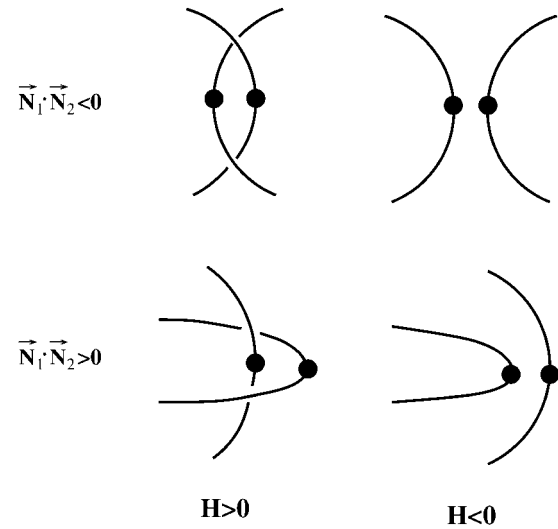

FIGURE 8 Schematics of representative juxtapositions belonging to different geometric regimes as defined by the parameters in Fig. 7.

center beads of the two segments of the given juxtaposition. The definition of curvature vectors in Fig. 7 is designed to be applied to lattice juxtapositions, and reduces to the usual definition of curvature vector in the continuum limit. We note that the discretized curvature vectors $\vec{N}_1$, $\vec{N}_2$ and the relative position vectors $\vec{r}_{12}$, $\vec{r}_{21}$ in our formulation are essentially equivalent, respectively, to the r_1, r_2 and p_{12}, p_{21} vectors in Buck and Zechiedrich (37). Similar to the
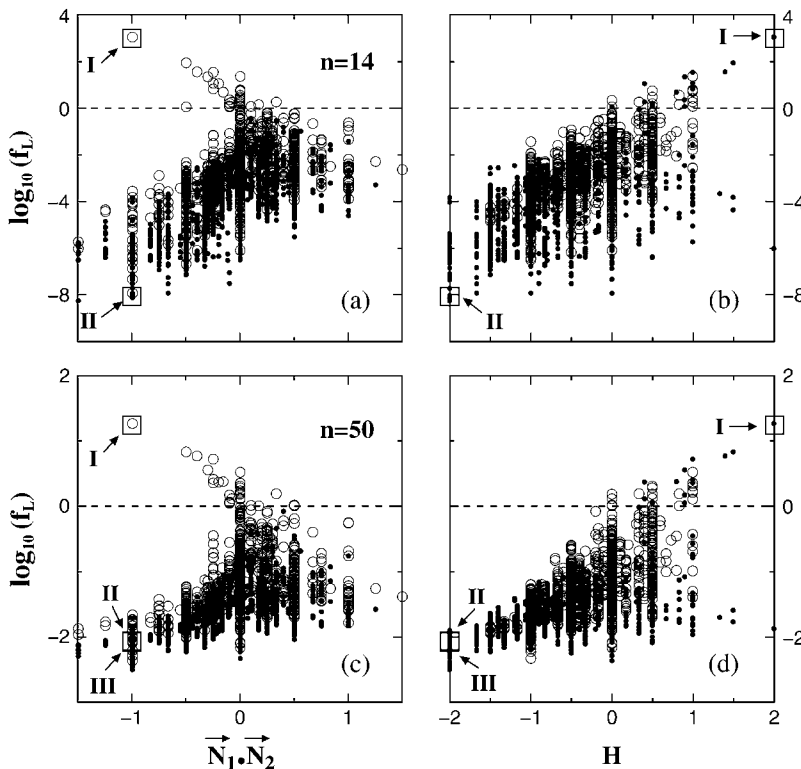

FIGURE 9 Correlation between global topology and local juxtaposition geometry. The discrimination factors f_L of all 2,982 possible 5 mer-on-5 mer juxtapositions are analyzed for loop sizes $n = 14$ (*upper panels*) and $n = 50$ (*lower panels*). (*a* and *c*) Scatter plots for $\vec{N}_1 \cdot \vec{N}_2$, where juxtapositions with $H \geq 0$ and $H < 0$ are represented, respectively, by open circles and solid dots. (*b* and *d*) Scatter plots for H, where juxtapositions with $\vec{N}_1 \cdot \vec{N}_2 \geq 0$ and $\vec{N}_1 \cdot \vec{N}_2 < 0$ are represented, respectively, by open circles and solid dots. The horizontal dashed lines mark the $f_L = 1$ level, i.e., juxtapositions at this level have equal numbers of linked and unlinked two-loop configurations. Data for $n = 14$ in *a* and *b* are obtained by exact enumeration, whereas those for $n = 50$ in *c* and *d* are by Monte Carlo sampling using 5×10^8 attempted chain moves for each data point. Large squares with incoming arrows marked by I, II, and III, are, respectively, data points for the hooked and free juxtapositions in Fig. 1. Data points for the free (nonplanar) juxtaposition (III) does not appear in the $n = 14$ plots because it is one of 32 juxtapositions with $f_L = 0$ for $n = 14$ (and hence its $\log f_L \to -\infty$).

formulation described in Fig. 1 of Buck and Zechiedrich (37), Fig. 8 shows how the $\vec{N}_1 \cdot \vec{N}_2$ and H parameters may be used to classify juxtaposition geometry. For instance, $\vec{N}_1 \cdot \vec{N}_2 < 0$, $H > 0$ corresponds to a general hook-like geometry, whereas $\vec{N}_1 \cdot \vec{N}_2 < 0$, $H < 0$ corresponds to free juxtapositions with the two segments curving away from each other.

We compute these geometrical parameters for all 2,982 5 mer-on-5 mer juxtapositions. Fig. 9 shows the variation of f_L as a function of the geometrical characteristics of a juxtaposition. Several features in these plots are noteworthy. First, consistent with the findings in Figs. 3–5, the diversity in f_L values are much higher for small loops ($n = 14$, *upper panels*) than for larger loops ($n = 50$, *lower panels*). Nonetheless, the general trend of the scatter plots for small loops is remarkably similar to that for the larger loop; and even for $n = 50$, the diversity of f_L values, which cover more than three orders of magnitude, remains significant. Second, most juxtapositions have $f_L < 1$ (log $f_L < 0$), implying that for most juxtapositions, the underlying two-loop configuration is more likely unlinked than linked. These data are consistent with the result for the 1 mer-on-1 mer control case in Fig. 4, and cast doubt on the commonplace notion that random segment passage would result in essentially equal probabilities for catenation and decatenation. These data also suggest that for a segment passage to favor decatenation rather than catenation, a far-from-random effort to select juxtapositions with $f_L > 1$ would be necessary. Third, although high positive values of log f_L are found among hooked-like geometries (Fig. 8, *upper left drawing*), not all such geometries behave similarly; indeed many of them have log $f_L < 0$ (*open circles* in Fig. 9, *a* and *c*, with $\vec{N}_1 \cdot \vec{N}_2 < 0$, and *solid dots* in Fig. 9, *b* and *d*, with $H > 0$). Fourth, the three hooked and free juxtapositions in Fig. 1 are situated at or near extreme positions on the scatter plots in Fig. 9, attaining maximum and near-minimum values of f_L among all 2,982 juxtapositions (the I, II, and III labels in Fig. 9). This observation confirms our intuition that these specific hooked and free juxtaposition geometries are rich in topological information content (37).

CONCLUDING REMARKS

In summary, we have shown that juxtapositions of certain geometries can embody highly significant information about the topological state of the much larger polymer configuration to which the given juxtaposition belongs. Our coarse-grained model findings lend credence to the theoretical argument that acting selectively on hooked juxtapositions is a possible mechanism by which type 2 topoisomerases disentangle DNA (37). Whether and how topoisomerases might have actually exploited the general physical principles elucidated here, however, are questions to be settled ultimately by experiments. To attain a closer match between theory and experiment, many issues remain to be addressed, some of which

may require a more detailed account of the physico-chemical properties of the polymer or biomolecule of interest. These open questions notwithstanding, our work establishes that statistically successful inferences from local juxtaposition geometry to global topology is a viable proposition in polymer physics.

The actions of topoisomerases and their apparent ability to discriminate global topological states have been poetically likened (31,34) to that of Maxwell's demon (63). Now, by focusing on the information content of juxtapositions, the results here demonstrate at an even more fundamental level that the statistical mechanical principles of Boltzmann may go a long way toward providing the necessary information for a topoisomerase's feat. A natural extension of this investigation would be to apply our approach to knotting and other forms of entanglement. Effort in that direction is under way.

REFERENCES

1. Sumners, D. W., and S. G. Whittington. 1988. Knots in self-avoiding walks. *J. Phys. A.-Math. Gen.* 21:1689–1694.

2. Lickorish, W. B. R. 1997. An Introduction to Knot Theory. Springer-Verlag, New York.

3. Buck, G. 1998. Four-thirds power law for knots and links. *Nature*. 392:238–239.

4. Gambini, R., and J. Pullin. 2000. Loops, Knots, Gauge Theories and Quantum Gravity. Cambridge University Press, Cambridge, UK.

5. Ladd, A. M., and L. E. Kavraki. 2004. Using motion planning for knot untangling. *Int. J. Robot Res.* 23:797–808.

6. Frisch, H. L., and E. Wasserman. 1961. Chemical topology. *J. Am. Chem. Soc.* 83:3789–3795.

7. Burchard, W. 1986. Theory of cyclic macromolecules. *In* Cyclic Polymers. J. A. Semlyen, editor. Elsevier, New York. 43–84.

8. ten Brinke, G., and G. Hadziioannou. 1987. Topological constraints and their influence on the properties of synthetic macromolecular systems. 1. Cyclic macromolecules. *Macromolecules*. 20:480–485.

9. de Gennes, P.-G. 1984. Tight knots. *Macromolecules*. 17:703–704.

10. Doi, M., and S. F. Edwards. 1986. The Theory of Polymer Dynamics. Oxford University Press, New York.

11. Dobay, A., J. Dubochet, K. Millett, P. E. Sottas, and A. Stasiak. 2003. Scaling behavior of random knots. *Proc. Natl. Acad. Sci. USA*. 100: 5611–5615.

12. Matsuda, D., A. Yao, H. Tsukahara, T. Deguchi, K. Furuta, and T. Inami. 2003. Average size of random polygons with fixed knot topology. *Phys. Rev. E*. 68:011102.

13. Moore, N. T., R. C. Lua, and A. Y. Grosberg. 2004. Topologically driven swelling of a polymer loop. *Proc. Natl. Acad. Sci. USA*. 101: 13431–13435.

14. Delbrück, M. 1962. Knotting problems in biology. *In* Mathematical Problems in the Biological Sciences (Proc. Symposia Applied

Mathematics, Vol. 14). American Mathematical Society, Providence, RI. 55–63.

15. Taylor, W. R., B. Xiao, S. J. Gamblin, and K. Lin. 2003. A knot or not a knot? SETting the record 'straight' on proteins. *Comput. Biol. Chem.* 27:11–15.

16. Liang, C., and K. Mislow. 1995. Topological features of protein structures: knots and links. *J. Am. Chem. Soc.* 117:4201–4213.

17. Taylor, W. R. 2000. A deeply knotted protein structure and how it might fold. *Nature.* 406:916–919.

18. Nureki, O., K. Watanabe, S. Fukai, R. Ishii, Y. Endo, H. Hori, and S. Yokoyama. 2004. Deep knot structure for construction of active site and cofactor binding site of tRNA modification enzyme. *Structure.* 12:593–602.

19. Zhou, H.-X. 2004. Loops, linkages, rings, catenanes, cages, and crowders: entropy-based strategies for stabilizing proteins. *Acc. Chem. Res.* 37:123–130.

20. Mallam, A. L., and S. E. Jackson. 2005. Folding studies on a knotted protein. *J. Mol. Biol.* 346:1409–1421.

21. Wasserman, S. A., and N. R. Cozzarelli. 1986. Biochemical topology: applications to DNA recombination and replication. *Science.* 232:951–960.

22. Wang, J. C. 1996. DNA topoisomerases. *Annu. Rev. Biochem.* 65:635–692.

23. Wang, J. C., and N. Davidson. 1966. Thermodynamic and kinetic studies on interconversion between linear and circular forms of phage lambda DNA. *J. Mol. Biol.* 15:111–123.

24. Pulleyblank, D. E., M. Shure, D. Tang, J. Vinograd, and H. P. Vosberg. 1975. Action of nicking-closing enzyme on supercoiled and non-supercoiled closed circular DNA: formation of a Boltzmann distribution of topological isomers. *Proc. Natl. Acad. Sci. USA.* 72:4280–4284.

25. Shaw, S. Y., and J. C. Wang. 1993. Knotting of a DNA chain during ring-closure. *Science.* 260:533–536.

26. Rybenkov, V. V., A. V. Vologodskii, and N. R. Cozzarelli. 1997. The effect of ionic conditions on the conformations of supercoiled DNA. 2. Equilibrium catenation. *J. Mol. Biol.* 267:312–323.

27. Wang, J. C. 1971. Interaction between DNA and an *Escherichia coli* protein ω. *J. Mol. Biol.* 55:523–533.

28. Berger, J. M., S. J. Gamblin, S. C. Harrison, and J. C. Wang. 1996. Structure and mechanism of DNA topoisomerase II. *Nature.* 379:225–232 (Erratum: 380:179 (1996)).

29. Roca, J., J. M. Berger, S. C. Harrison, and J. C. Wang. 1996. DNA transport by a type II topoisomerase: direct evidence for a two-gate mechanism. *Proc. Natl. Acad. Sci. USA.* 93:4057–4062.

30. Rybenkov, V. V., C. Ullsperger, A. V. Vologodskii, and N. R. Cozzarelli. 1997. Simplification of DNA topology below equilibrium values by type II topoisomerases. *Science.* 227:690–693.

31. Pulleyblank, D. E. 1997. Of topo and Maxwell's dream. *Science.* 277:648–649.

32. Yan, J., M. O. Magnasco, and J. F. Marko. 1999. A kinetic proof-reading mechanism for disentanglement of DNA by topoisomerases. *Nature.* 401:932–935.

33. Yan, J., M. O. Magnasco, and J. F. Marko. 2001. Kinetic proofreading can explain the suppression of supercoiling of circular DNA molecules by type-II topoisomerases. *Phys. Rev. E.* 63:031909.

34. Vologodskii, A. 1998. Maxwell demon and topology simplification by type II topoisomerases. *In* RECOMB 98: Proc. Int. Conf. Computational Molecular Biology, 2nd. Association for Computing Machinery, New York. 266–269.

35. Vologodskii, A. V., W. Zhang, V. V. Rybenkov, A. A. Podtelezhnikov, D. Subramanian, J. D. Griffith, and N. R. Cozzarelli. 2001. Mechanism of topology simplification by type II DNA topoisomerases. *Proc. Natl. Acad. Sci. USA.* 98:3045–3049.

36. Trigueros, S., J. Salceda, I. Bermudez, X. Fernández, and J. Roca. 2004. Asymmetric removal of supercoils suggests how topoisomerase II simplifies DNA topology. *J. Mol. Biol.* 335:723–731.

37. Buck, G. R., and E. L. Zechiedrich. 2004. DNA disentangling by type-2 topoisomerases. *J. Mol. Biol.* 340:933–939.

38. Zechiedrich, E. L., and N. Osheroff. 1990. Eukaryotic topoisomerases recognize nucleic acid topology by preferentially interacting with DNA crossovers. *EMBO J.* 9:4555–4562.

39. Corbett, K. D., A. J. Schoeffler, N. D. Thomsen, and J. M. Berger. 2005. The structural basis for substrate specificity in DNA topoisomerase IV. *J. Mol. Biol.* 351:545–561.

40. Germe, T., and O. Hyrien. 2005. Topoisomerase II-DNA complexes trapped by ICRF-193 perturb chromatin structure. *EMBO Rep.* 6:729–735.

41. Zechiedrich, E. L., A. B. Khodursky, and N. R. Cozzarelli. 1997. Topoisomerase IV, not gyrase, decatenates products of site-specific recombination in *Escherichia coli. Genes Dev.* 11:2580–2592.

42. Deibler, R. W., S. Rahmati, and E. L. Zechiedrich. 2001. Topoisomerase IV, alone, unknots DNA in *E. coli. Genes Dev.* 15:748–761.

43. Orr, W. J. C. 1947. Statistical treatment of polymer solutions at infinite dilution. *Trans. Faraday Soc.* 43:12–27.

44. Domb, C. 1969. Self avoiding walks on lattices. *Adv. Chem. Phys.* 15:229–259.

45. Barber, M. N., and B. W. Ninham. 1970. Random and Restricted Walks: Theory and Applications. Gordon and Breach, New York.

46. Lim, H. A. 1992. Mathematical formulations and computer enumerations of polymer models with loops. *Int. J. Mol. Phys.* 3:385–446.

47. de Gennes, P.-G. 1979. Scaling Concepts in Polymer Physics. Cornell University Press, Ithaca, NY.

48. Freed, K. F. 1987. Renormalization Group Theory of Macromolecules. Wiley, New York.

49. Soteros, C. E., D. W. Sumners, and S. G. Whittington. 1992. Entanglement complexity of graphs in Z^3. *Math. Proc. Camb. Philos. Soc.* 111:75–91.

50. Orlandini, E., M. C. Tesi, S. G. Whittington, D. W. Sumners, and E. J. Janse van Rensburg. 1994. The writhe of a self-avoiding walk. *J. Phys. A.-Math. Gen.* 27:L333–L338.

51. Yao, A., H. Tsukahara, T. Deguchi, and T. Inami. 2004. Distribution of the distance between opposite nodes of random polygons with a fixed knot. *J. Phys. A.-Math. Gen.* 37:7993–8006.

52. Chan, H. S., and K. A. Dill. 1989. Intrachain loops in polymers: effects of excluded volume. *J. Chem. Phys.* 90:492–509 (Errata: 96:3361 (1992); 107:10353 (1997)).

53. Chan, H. S., and K. A. Dill. 1990. The effects of internal constraints on the configurations of chain molecules. *J. Chem. Phys.* 92:3118–3135 (Erratum: 107:10353 (1997)).

54. Chan, H. S., and K. A. Dill. 1989. Compact polymers. *Macromolecules.* 22:4559–4573.

55. Chan, H. S., and K. A. Dill. 1990. Origins of structure in globular proteins. *Proc. Natl. Acad. Sci. USA.* 87:6388–6392.

56. Chan, H. S., and K. A. Dill. 1991. Polymer principles in protein structure and stability. *Annu. Rev. Biophys. Biophys. Chem.* 20:447–490.

57. Tadokoro, H. 1979. Structure of Crystalline Polymers. Wiley, New York.

58. Flammini, A., A. Maritan, and A. Stasiak. 2004. Simulations of action of DNA topoisomerases to investigate boundaries and shapes of spaces of knots. *Biophys. J.* 87:2968–2975.

59. Fourey, S., and R. Malgouyres. 2001. A digital linking number for discrete curves. *Int. J. Pattern Recogn.* 15:1053–1074.

60. Madras, N., A. Orlitsky, and L. A. Shepp. 1990. Monte Carlo generation of self-avoiding walks with fixed endpoints and fixed length. *J. Stat. Phys.* 58:159–183.

61. Ullsperger, C., and N. R. Cozzarelli. 1996. Contrasting enzymatic activities of topoisomerase IV and DNA gyrase from *Escherichia coli. J. Biol. Chem.* 271:31549–31555.

62. Vologodskii, A., and N. R. Cozzarelli. 1996. Effect of supercoiling on the juxtaposition and relative orientation of DNA sites. *Biophys. J.* 70:2548–2556.

63. Maxwell, J. C. 1871. Theory of Heat. Longmans Green, London, UK.